Research Article

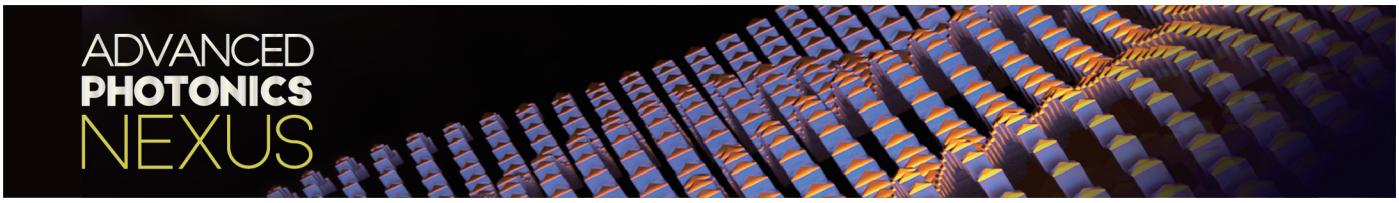

Supercontinuum generation using long-period-grating waveguides on silicon

Hongzhi Xiong,[a] Xinmin Yao,[a] Qingrui Yao,[a] Qingbo Wu,[a] Hongyuan Cao,[a] Yaoxin Bao,[a] Fei Huang,[a] Zejie Yu,[a] Ming Zhang,[b] and Daoxin Dai[a,b,*]

[a]Zhejiang University, College of Optical Science and Engineering, International Research Center for Advanced Photonics, State Key Laboratory for Modern Optical Instrumentation, Center for Optical and Electromagnetic Research, Hangzhou, China
[b]Zhejiang University, Ningbo Research Institute, Ningbo, China

Abstract. Research on supercontinuum sources on silicon has made significant progress in the past few decades. However, conventional approaches to broaden the spectral bandwidth often rely on complex and critical dispersion engineering by optimizing the core thickness or introducing the cladding with special materials and structures. We propose and demonstrate supercontinuum generation using long-period-grating (LPG) waveguides on silicon with a C-band pump. The LPG waveguide is introduced for quasi-phase matching, and the generated supercontinuum spectrum is improved greatly with grating-induced dispersive waves. In addition, the demonstrated LPG waveguide shows a low propagation loss comparable with regular silicon photonic waveguides without gratings. In experiments, when using a 1550-nm 75-fs pulse pump with a pulse energy of 200 pJ, the supercontinuum spectrum generated with the present LPG waveguide shows an ultrabroad extent from 1150 to 2300 nm, which is much wider by 200 nm than that achieved by dispersion-engineered uniform silicon photonic waveguides on the same chip. This provides a promising option for on-chip broadband light source for silicon photonic systems.

Keywords: silicon photonics; supercontinuum generation; nonlinear optics; waveguide grating.

Received Jul. 29, 2024; revised manuscript received Oct. 12, 2024; accepted for publication Dec. 5, 2024; published online Jan. 24, 2025.

[DOI: 10.1117/1.APN.4.1.016014]

1 Introduction

Supercontinuum generation (SCG) is a phenomenon in which an ultrashort and intense pulse experiences significant spectral broadening when propagating in a nonlinear optical material/structure. Recent work has extensively explored SCGs with various optical waveguides based on silicon,[1] Si_3N_4,[2–7] silica,[8] lithium niobate,[9–17] and chalcogenide fibers.[18,19] Among them, silicon photonic waveguides offer the advantages of broad transparent windows and complementary metal oxide semiconductor (CMOS) compatibility.[20,21] In 2014, Leo et al.[1] reported SCG ranging from 1.1 to 1.7 μm on a silicon-on-insulator (SOI) platform with a 150-fs pulsed pump source with the wavelength centered at 1.55 μm. The first octave-spanning SCG in silicon waveguides with a 2.5-μm pump was also demonstrated in the same year.[22] In 2018, Nader et al.[23] reported that the mid infrared (MIR) SCG using a silicon-on-sapphire optical waveguide pumped by a 100-fs pulsed source with the wavelength centered at 3.06 μm. Kou et al.[24] also reported the MIR SCG ranging from 2 to 5 μm with a suspended silicon photonic waveguide by utilizing a 300-fs pulsed pump source around 4 μm. In 2024, Boukar et al.[25] reported the numerical study of the supercontinuum phenomenon raised from Airy pulses.

To broaden the SCG bandwidth, dispersion engineering was extensively employed. However, for the most popular standard silicon photonic waveguide, which usually has a thickness of 220 nm, the dispersion property is not as satisfactory as what is desired for SCG, resulting in low spectral energy, especially in the wavelength range beyond 2 μm. Previously, there were some works that attempted to address this issue by increasing the core layer thickness to be more than 220 nm[26–28] or by introducing some special cladding.[28] These approaches, however, make the structure/processes of the SCG chip incompatible with the standardized silicon photonics.

*Address all correspondence to Daoxin Dai, dxdai@zju.edu.cn

In addition to dispersion engineering, several alternative physical mechanisms have also been explored to improve SCG spectra. Among them, varying the dispersion profile of a waveguide has significant promise. Some works were reported with simple tapered waveguides to vary the dispersion. In 2019, Singh et al.[29] presented width-varying waveguides on silicon, enabling 16-dB signal enhancement and wavelength extension of 100 nm in the 1550-nm window when compared with a fixed-dispersion waveguide. In 2023, Torre et al.[30] reported mid-infrared SCG in a tapered Si–Ge waveguide. Moreover, complex waveguide profiles in the propagation direction were used and usually designed by the optimization method or algorithm. In 2020, Wei et al.[31] reported SCG assisted by wave trapping in dispersion-managed silicon photonic waveguides. In 2023, Zia et al.[32] reported SCG from sign-alternating-dispersion waveguides on Si_3N_4. More recently, Lee et al.[33] reported the SCG realized using inverse-designed freeform Si_3N_4 waveguides.

Moreover, the periodic-structure-assisted broadband phase-matching method holds significant promise. In 2017, Hickstein et al.[34] experimentally demonstrated a quasi-phase-matched SCG with the TE_{20} and TE_{00} modes in Si_3N_4 optical waveguides. However, the generated spectra are mixed with different optical transverse modes, which is not easy to couple and becomes challenging in real applications such as optical coherence tomography (OCT) or optical communications. In addition, the grating also causes frequency conversion among different modes, which further lowers the energy carried by the fundamental mode.

The grating structure also has a much higher loss than the uniform optical waveguide (without grating). In 2021, Singh et al.[35] introduced a silicon Bragg grating through periodic deposition of charge carriers.[20] Although they tried to weaken the Bragg reflection using a weak grating, the reflection remained more than 90% at quasi-phase-matched wavelengths. Consequently, a significant portion of the SCG light was reflected. Moreover, the spectrum of SCG is almost the same as that generated with an undoped waveguide, except that a single narrow peak is generated around 1220 nm. Such a weak grating also has less transfer efficiency, and the carrier doping also introduces some additional losses. Because the index changing is small, the grating-induced dispersive wave is not yet strong.

In this work, we propose and demonstrate long-period-grating (LPG) waveguides for SCG on silicon with a C-band pump. Unlike previous works using waveguides without gratings,[1,28] we introduce LPG waveguides for quasi-phase matching to improve the SCG. Here, the entire spectrum is generated with the fundamental mode (TE_{00}), eliminating the need for additional mode manipulating or mode purification, which thus greatly simplifies the device fabrication and reduces the loss as well. Compared with previous silicon SCGs based on gratings,[34,35] the present work achieves improved spectral characteristics with broader, stronger, and more concentrated dispersive waves beyond 2 μm. Notably, the present LPG waveguide shows an ultrabroad extent from 1150 to 2300 nm, which is much wider by 200 nm than that achieved by conventional dispersion-engineered silicon photonic waveguides on the same chip. This spectral broadening is enhanced, even without requiring any special materials, so that it is compatible with the standard structure/processes of silicon photonics. In addition, the long grating period facilitates the structure to be adiabatic, resulting in minimal linear loss comparable with the regular uniform waveguides without gratings. Furthermore, the Bragg reflection in the present waveguide structure is very weak, which helps to improve overall efficiency. These key features make the present approach highly attractive and potentially valuable for applications in spectroscopy and imaging systems.

2 Design of LPG Waveguides for SCG

Here, an SOI wafer with a 220-nm-thick silicon core layer and a 3 μm-thick buried-oxide layer is used. Figure 1(a) schematically illustrates the proposed LPG waveguide based on triangular corrugations with a period of Λ and a corrugation depth of δ. As the period Λ of the LPG is >100 μm, the grating becomes almost adiabatic, and the linear propagation loss is nearly the same as the uniform waveguides ($\delta = 0$). Figure 1(b) schematically illustrates the theory of the grating-induced phase matching. Unlike traditional Bragg gratings, which are designed to realize

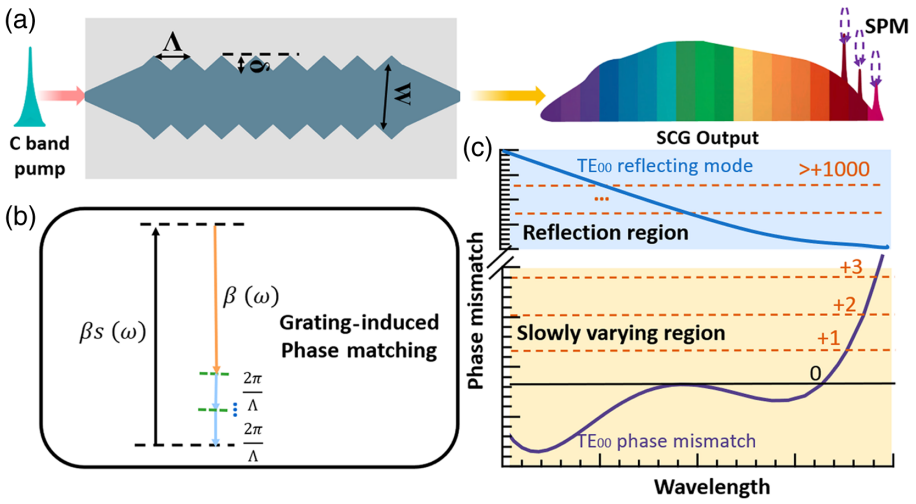

Fig. 1 (a) Design of LPG waveguides. (b) Diagram of grating-induced phase matching. The soliton wave and dispersive wave are quasi-phase-matched and cause grating-induced phase matching. (c) Using LPG waveguides, the TE_{00} phase mismatch intersects the grating-induced phase mismatch, so the matching condition is achieved, and a spectrum with several peaks is generated.

the phase matching between the optical transverse modes with different orders or directions, here, the present LPG is designed to realize the phase matching between the soliton and quasi-plane wave of the same TE_{00} mode. When the phase mismatch intersects with the grating-induced phase mismatch, the matching condition is satisfied, and a grating-induced dispersive wave is generated at this frequency accordingly. The frequency of grating-induced dispersive waves is calculated by[36]

$$\beta_s(\omega) - \beta(\omega) = \frac{2\pi}{\Lambda} m, \tag{1}$$

where $m = 0, \pm 1, \pm 2, \ldots, \omega$ is the angular frequency of the grating-induced dispersive wave, and $\beta_s(\omega)$ is the soliton wave vector given as

$$\beta_s(\omega) = \beta(\omega_s) + (\omega - \omega_s)\beta_1(\omega_s) + \gamma P/2, \tag{2}$$

in which P is the peak power of the first ejected soliton, ω_s is the frequency of the soliton frequency, γ is the nonlinear coefficient, and $\beta_1(\omega_s)$ is the first-order dispersion coefficient at ω_s.

As the core width is changing for the present LPG waveguides, the effective index is a function of the propagation distance. Hence, we use the effective dispersion D_{eff} and the effective phase mismatch $\beta_{1,\text{eff}}$, which are given as

$$D_{\text{eff}} = \frac{1}{\Lambda}\int_0^{\Lambda} D(l)\mathrm{d}l, \tag{3}$$

$$\beta_{1,\text{eff}} = \frac{1}{\Lambda}\int_0^{\Lambda} \beta_1(l)\mathrm{d}l, \tag{4}$$

where D is the dispersion of the waveguide and l is the propagation length in a single period. As the core width of the LPG waveguide varies with the propagation distance, D and β_1 also depend on the propagation distance.

Previous grating-based SCG on silicon[35] was designed for the +1-order phase-matching wavelength in the reflection region, as shown in Fig. 1(c), which results in a Bragg-grating forbidden band overlapping with the generated SCG spectrum.[35] Even though this issue can be alleviated by employing a weak Bragg-grating waveguide with depositing charge carriers, the reflection remains significant (even exceeding 90%).[35] In contrast, our LPG design generates dispersive waves, relying on quasi-phase matching within the slowly varying region, which offers three key advantages. First, the matching order of the TE_{00} reflection modes is even more than 1000, and the total periods are fewer than 20. Consequently, Bragg reflection becomes negligible across the entire spectrum in our case. Second, the increased Bragg period from micrometers to sub-millimeters ensures an adiabatic structural design, mitigating Bragg-grating-induced propagation losses (as verified in experiments below). As shown in Fig. S1 in the Supplementary Material, the simulated Bragg reflection is close to 100% in the Bragg forbidden band for conventional Bragg grating waveguides. For the present LPG waveguide, the transmission is higher than 99.99% according to the simulation. Another challenge in the grating waveguide for SCG is grating-induced mode conversion among different modes in the propagation direction, which makes the modes complex and difficult to convert to the fundamental mode. The mode converting is almost impossible to avoid in the TE_{00}-pumped and TE_{20}-supported SCG waveguides, which are the conditions in previous works.[28,34] In Fig. S2 in the Supplementary Material, we simulate the TE_{00} and TE_{20} mode coupling in the grating structure, showing a complex spectrum mixed with a different order of modes. It should be noted that as the generated spectrum is so broadband, it is almost impossible to avoid mode converting for all the wavelengths. As a result, we choose 220-nm-thick strip silicon photonic waveguides and make the single-mode condition satisfied for the pump wavelengths, whereas for the shortest wavelengths, not only the TE_{00}/TM_{00} mode but also the TE_{10} and TM_{10} modes are supported, as shown in Fig. S2(c) in the Supplementary Material. As a result, with the present symmetric LPG waveguide, all the generated SC light is in the TE_{00} mode.

Figures 2(a) and 2(b) show the results of the dispersion and phase mismatch of the uniform waveguides (i.e., $\delta = 0$) with a core width of $W = 525$, 550, 575, 600, and 625 nm. As can be seen, the waveguide has anomalous dispersion when the width is chosen within the range of 525 to 600 nm when the pump wavelength is 1550 nm. Figures 2(c) and 2(d) show the calculated results of the dispersion and phase mismatch for the waveguides designed with $W = 550$ nm and $\delta = 100$, 200, 300, and 400 nm. As can be seen, D becomes smaller as δ increases, whereas D becomes less than 0 when δ comes to 400 nm. Although the waveguide with larger δ has a stronger interaction between the pump and the grating-induced dispersive waves, the soliton fission length becomes larger when D becomes smaller, and thus, δ should be chosen appropriately to enhance the grating-induced dispersive waves.

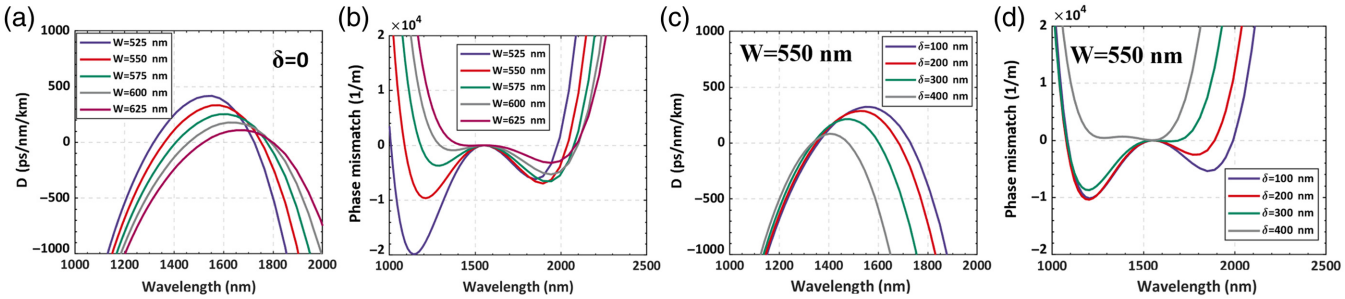

Fig. 2 (a), (b) Dispersion and phase mismatch of uniform ($\delta = 0$) waveguides at different widths of $W = 525$, 550, 575, 600, and 625 nm. (c), (d) Dispersion and phase mismatch of LPG waveguides at $W = 550$ nm and $\delta = 100$, 200, 300, and 400 nm. In all simulations, it is a strip waveguide with height = 220 nm.

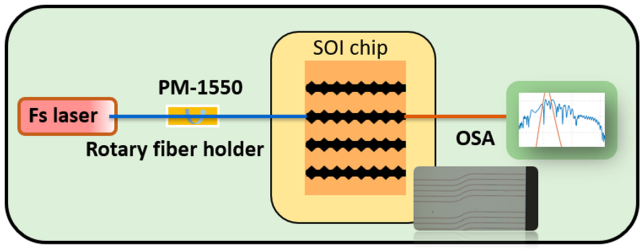

Fig. 3 Measurement setup. OSA, optical spectrum analyzer. Inset: microscope image of the fabricated silicon photonic LPG waveguides.

3 Result

3.1 SCG in LPG Waveguides

In our experiment, we first used a 1550-nm 230-fs pulse pump with a pulse energy of 200 pJ on the chip. The experimental setup is shown in Fig. 3, where a mode-locked Er-fiber laser oscillator produces optical pulses with a center wavelength of 1550 nm at a repetition rate of 100 MHz. The optical pulses are then delivered through a length-designed polarization-maintaining fiber (PM 1550), and the polarization is set to the TE mode with the help of a rotary fiber holder. On the output side, the spectrum is collected by a small-mode-size fiber and then sent to an optical spectrum analyzer (OSA). Figure 4(a) shows the output spectra measured for the cases with $W = 525$, 550, 575, 600, and 625 nm. It can be seen that the 550-nm-wide silicon photonic waveguide enables the SCG with a bandwidth from ~1330 to 1990 nm. The waveguide loss is measured to be ~5 dB/cm using the cut-back methods. It should be noted that with a shorter pulse duration and higher pulse power, the bandwidth could be extended further. When comparing the SCGs in different waveguides, the pulse energy and the pulse duration should be the same. Figure 4(b) shows the output spectra of the present LPG waveguides designed with $\Lambda = 0.5$ mm, $W = 550$ nm, and $\delta = 100$, 200, and 300 nm. It can be seen that the LPG-induced dispersive waves have different wavelengths when varying δ, mainly because larger δ has a larger phase mismatch, as shown in Fig. 2(d). When $\delta = 100$ nm, the quasi-phase matching grating-induced dispersive waves are not obvious, mainly because the grating is weak and the efficiency is low. Figure 4(c) plots the output spectrum of the LPG waveguides designed with $W = 550$ nm, $\delta = 200$ nm, and $\Lambda = 1$, 0.5, 0.3, and 0.1 mm. It can be seen that the grating-induced dispersive waves are too weak to be seen when $\Lambda = 0.1$ mm. On the other hand, when $\Lambda = 1$ mm, the peaks of the grating-induced dispersive waves are too close to be distinguished. For the case with $\Lambda = 0.5$ mm (0.3 mm), the +1 and +2-order grating-induced dispersive waves are located at wavelengths 1982 nm (2033 nm) and 2051 nm (2100 nm), respectively.

Figure 5(a) shows the generated spectra in the LPG waveguides with $W = 550$ nm, $\delta = 200$ nm, and $\Lambda = 0.3$ mm when the pulse energy increases from 2 to 10 dBm. To give a comparison, the measured results for the 550-nm-wide uniform silicon photonic waveguide are also given, as shown in Fig. 5(b). In this experiment, the input coupling loss is excluded. Generally speaking, the bandwidth increases with the average pump power. It can be seen that the +1 grating-induced dispersive wave can still be detected when the average power is only 7 dBm. Moreover, these spectra shown in Fig. 5(a) are obviously wider than those generated in the uniform waveguide shown in Fig. 5(b), particularly when the pump power is relatively low (e.g., 2 and 5 dBm). The main reason is that the LPG waveguide has near-zero $\beta_{1,\mathrm{eff}}$ in these wavelengths, which is not achievable for the 550-nm-wide uniform waveguide.

3.2 Continuing SCG for LPG Waveguides

To demonstrate the ultrabroad bandwidth, we use a 75-fs 1550-nm pump with 100 pJ pulse energy, and the LPG waveguide with the parameters of $W = 550$ nm, $\delta = 300$ nm, and $\Lambda = 1$ mm. The parameters δ and W are chosen according to the principle that the tooth depths should be larger to get stronger dispersive waves while ensuring anomalous dispersion. Figures 6(a) and 6(b) show the simulated temporal and spectral evolution along a 7-mm-long silicon LPG waveguide. Unlike those previous simulation works, which include only the SCG waveguides,[1,28] the pulse-broadening happening in the butt-coupler is considered in our simulation to be more accurate. The butt coupler is a 200-μm-long inverse taper with a core width that varies linearly from 180 to 250 nm. As shown in

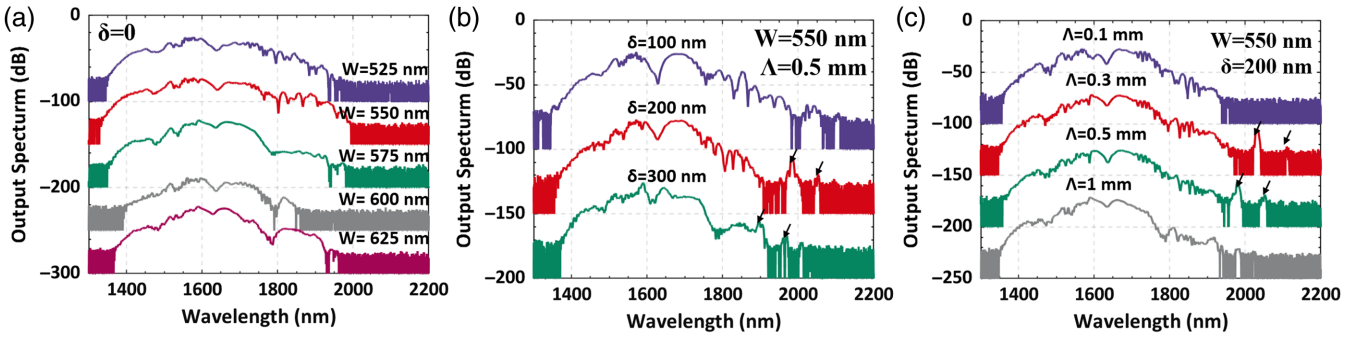

Fig. 4 (a) Measured SCG output spectra of uniform ($\delta = 0$) waveguides, with different waveguide widths. (b) Measured SCG output spectra when varying δ, where $W = 550$ nm and $\Lambda = 0.5$ mm. (c) Measured SCG output spectra of LPG waveguides when varying Λ, where $W = 550$ nm and $\delta = 200$ nm. In all experiments, we use 1550 nm, 100-MHz repetition rate, and 230-fs pulses with an average power of 0.01 W. Spectra are vertically offset by multiples of 50 dB for clarity. The arrows indicate the grating-induced dispersive waves.

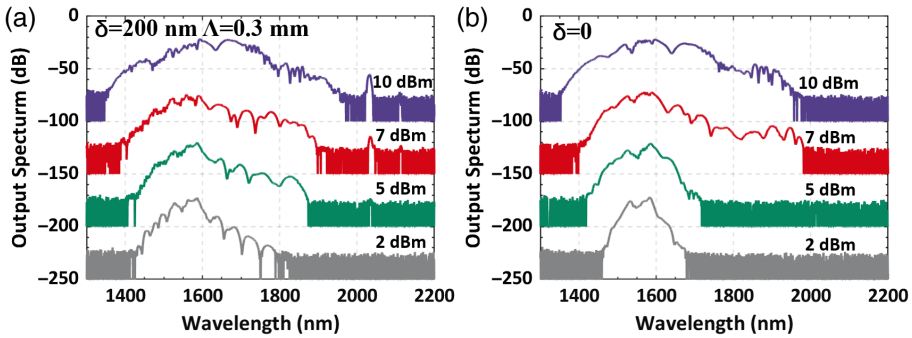

Fig. 5 (a) Measured SCG output spectra of the LPG waveguides with different average pump powers, where $W = 550$ nm, $\delta = 200$ nm, and $\Lambda = 0.3$ mm. (b) Measured SCG output spectra of 550-nm waveguide with different average pump powers. Spectra are vertically offset by multiples of 50 dB for clarity.

Fig. 6(a), the temporal simulation results show that the pulse is intensively broadened in the 200-μm-long region at the input end (i.e., $0 < z < 200$ μm), where the waveguide is narrower than 300 nm and thus has a huge normal dispersion. In contrast, when propagating in the grating region, the pulse is first compressed in the first period of the grating, whereas the spectrum is broadened to cover the range of 1300 to 1900 nm at the end of the first period (i.e., $z = 1000$ μm). Then, the soliton fission is observed at the location of $z \sim 1.2$ mm, where the pulse is intensively broadened both in the time and frequency domains. When 2 mm $< z <$ 7 mm, the spectrum width is almost unchanged, whereas the pulse width in the time domain continues to be broadened. The ripples in the time domain shown in Fig. 6(a) are mainly due to the periodic modulation of the group velocity in the LPG waveguide. The simulated output spectrum is as wide as 1.1 to 2.3 μm. Figure 6(c) shows the measured final output spectra from the present LPG waveguide and the 550-nm-wide uniform waveguide ($\delta = 0$). The simulation results are also shown in the figures (see the dashed lines). In the experiments, the continuing spectrum covering from 1150 to 2300 nm is obtained for the LPG waveguide, which is ~200 nm wider than that (1200 to 2150 nm) obtained from the uniform ($\delta = 0$) waveguide. As the LPG used here has a period as large as 1 mm, the grating-induced dispersive waves are so close to each other, and thus, we can achieve continued and flattened spectrum broadening rather than several separate peaks.

Table 1 gives a comparison of the reported works about SCG based on silicon, indicating that the present work features the

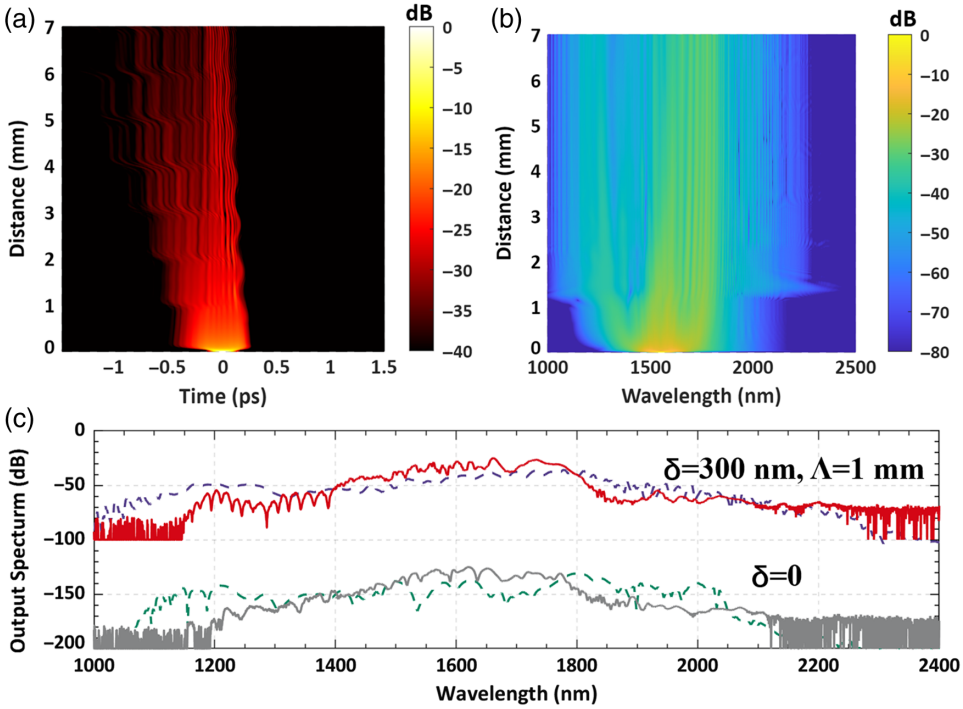

Fig. 6 (a) Simulated time and (b) spectral evolution on the LPG waveguides. (c) The output spectra of the SCG from the LPG waveguide and the uniform ($\delta = 0$) waveguide, respectively. Dashed lines: simulated results. Solid lines: experimental results. Spectra are vertically offset by 100 dB for clarity.

Table 1 Main parameters of silicon SCG.

Year	Ref.	λ_{pump} (nm)	Bandwidth (nm)	Pulse duration (fs)	Peak power (kW)	Platform, structure
2018	24	4000	2000 to 5000	300	42	500-nm suspended Si, uniform waveguide
2023	30	3900	2400 to 5500	200	2.37	Two-stage 3.3 μm Si–Ge waveguide
2018	27	1950	1060 to 2400	50	0.32	400-nm SOI, uniform waveguide
2017	28	1550	1060 to 2350	80	0.625	250-nm SOI, double-layer cladding
2014	1	1550	1100 to 1700	150	0.032	Standard 220-nm SOI, uniform waveguide
2024	25	1550	1300 to 1900	50	0.05	700-nm SOI, uniform waveguide, Airy pulse
2024	This work	1550	1200 to 2150	75	2.67	Standard 220-nm SOI, uniform waveguide
2024	This work	1550	1150 to 2300	75	2.67	Standard 220-nm SOI, LPG waveguide

most broadband spectrum among all with standard 220-nm SOI photonic waveguides pumped at the C band. Specifically, the spectra obtained by our LPG waveguide are >300 nm wider than that from the Bragg-grating SCG developed on silicon.[35] Note that the LPG waveguides SCG could be further improved when combined with other methods, such as introducing a thick-silicon photonic waveguide[26] for optimal dispersion, special cladding material/design[28] for dispersion/coupling improvement, or longer pump wavelength for smaller nonlinear loss.[27]

4 Conclusion

We have proposed and demonstrated on-chip SCG covering the range from 1.15 to 2.3 μm with a C-band pump laser by introducing LPG waveguides. We have introduced an LPG waveguide for quasi-phase matching to broaden the output spectrum. The wavelength location of these grating-induced dispersive waves can be designed according to the calculated effective dispersion. We have also obtained continuing and ultrabroad SCG covering the wavelength range of 1150 to 2300 nm (more than one octave) using 1550-nm 75-fs pulses with a pulse energy of 200 pJ. The obtained SCG bandwidth is 200 nm broader than that achieved with conventional dispersion-engineered silicon photonic waveguides on the same chip. Note that the SCG could be further broadened by shortening the butt coupler and lowering its dispersion. Moreover, instead of directly choosing the triangular corrugations, the inverse-designed corrugations may have further improved performances in obtaining high peak power and low pulse duration. Unlike previous works exhibiting high-order transverse modes,[34] the present SCG on silicon is with the TE_{00} mode so that the SCG spectrum can be collected by a single-mode fiber without additional mode conversion. The present LPG waveguide designed with a slowly varying grating corrugation can effectively suppress the spectrum reflection and mode conversion,[34,35] greatly reducing the reflection losses to near zero, which is even at the same level as the width-fixed waveguides or extremely slow varying but aperiodic waveguides.[32,33] Furthermore, the present on-chip SCG waveguides can be fabricated easily with standard foundry processes for passive silicon photonics. In summary, the proposed LPG waveguide structure provides an attractive option for realizing on-chip SCG sources.

5 Appendix: Supplementary Information

See the Supplementary Material for details of the simulated Bragg reflection of traditional Bragg grating SCG waveguides in Fig. S1 in the Supplementary Material, the simulated TE_{00} and TE_{20} mode coupling in the TE_{20} supported grating waveguide in Fig. S1(a) in the Supplementary Material, and the effective index of different modes as a function of wavelengths in a typical TE_{20} supported waveguide and our LPG waveguide in Figs. S2(b) and S2(c) in the Supplementary Material, respectively.

Disclosures

The authors declare no conflicts of interest.

Code and Data Availability

The data that support the findings of this study are available from the corresponding author upon reasonable request.

Acknowledgments

This work was supported by the National Major Research and Development Program (Grant No. 2022YFB2803800), the National Natural Science Foundation of China (Grant Nos. 91950205, 92150302, and U23B2047), the Zhejiang Provincial Natural Science Foundation (Grant No. LD19F050001), the Zhejiang Provincial Major Research and Development Program (Grant No. 2021C01199), the Leading Innovative and Entrepreneur Team Introduction Program of Zhejiang (Grant No. 2021R01001), and the Fundamental Research Funds for the Central Universities.

References

1. F. Leo et al., "Dispersive wave emission and supercontinuum generation in a silicon wire waveguide pumped around the 1550 nm telecommunication wavelength," *Opt. Lett.* **39**(12), 3623–3626 (2014).
2. S. Fatema et al., "Multiple mode couplings in a waveguide array for broadband near-zero dispersion and supercontinuum generation," *J. Lightwave Technol.* **39**(1), 216–222 (2021).
3. D. Grassani et al., "Mid infrared gas spectroscopy using efficient fiber laser driven photonic chip-based supercontinuum," *Nat. Commun.* **10**(1), 1553 (2019).
4. D. D. Hickstein et al., "Self-organized nonlinear gratings for ultrafast nanophotonics," *Nat. Photonics* **13**(7), 494–499 (2019).
5. M. A. G. Porcel et al., "Two-octave spanning supercontinuum generation in stoichiometric silicon nitride waveguides pumped at telecom wavelengths," *Opt. Express* **25**(2), 1542–1554 (2017).
6. Y. Fang et al., "Three-octave supercontinuum generation using SiO_2 cladded Si_3N_4 slot waveguide with all-normal dispersion," *J. Lightwave Technol.* **38**(13), 3431–3438 (2020).

7. M. R. Alizadeh et al., "Numerical investigation of supercontinuum generation and optical frequency combs in SiN-based PCF with high nonlinear coefficient," *Optoelectron. Lett.* **20**(3), 163–170 (2024).
8. G. Wang et al., "Stable high-peak-power fiber supercontinuum generation for adaptive femtosecond biophotonics," *Adv. Photonics Nexus* **3**(4), 046012 (2024).
9. Y. Okawachi et al., "Chip-based self-referencing using integrated lithium niobate waveguides," *Optica* **7**(6), 702–707 (2020).
10. M. Yu et al., "Coherent two-octave-spanning supercontinuum generation in lithium-niobate waveguides," *Opt. Lett.* **44**(5), 1222–1225 (2019).
11. S. Lauria et al., "Mixing second- and third-order nonlinear interactions in nanophotonic lithium-niobate waveguides," *Phys. Rev. A* **105**(4), 043511 (2022).
12. J. Lu et al., "Octave-spanning supercontinuum generation in nanoscale lithium niobate waveguides," *Opt. Lett.* **44**(6), 1492–1495 (2019).
13. M. Jankowski et al., "Ultrabroadband nonlinear optics in nanophotonic periodically poled lithium niobate waveguides," *Optica* **7**(1), 40–46 (2020).
14. Y. Jia et al., "Ion-cut lithium niobate on insulator technology: recent advances and perspectives," *Appl. Phys. Rev.* **8**(1), 011307 (2021).
15. G. Chen et al., "Advances in lithium niobate photonics: development status and perspectives," *Adv. Photonics* **4**(3), 034003 (2022).
16. M. G. Vazimali et al., "Applications of thin-film lithium niobate in nonlinear integrated photonics," *Adv. Photonics* **4**(3), 034001 (2022).
17. K. F. Fiaboe et al., "Mid-IR supercontinuum generation in a silicon nitride loaded lithium niobate on sapphire waveguide," *Photonics Nanostruct. – Fundam. Appl.* **60**, 101274 (2024).
18. A. Cheshmberah et al., "Design of all-normal dispersion with $Ge_{11.5}As_{24}Se_{64.5}/Ge_{20}Sb_{15}Se_{65}$ chalcogenide PCF pumped at 1300 nm for supercontinuum generation," *Opt. Quantum Electron.* **53**(8), 461 (2021).
19. A. Cheshmberah et al., "Supercontinuum generation in PCF with $As2S_3/Ge_{20}Sb_{15}Se_{65}$ chalcogenide core pumped at third telecommunication wavelengths for WDM," *Opt. Quantum Electron.* **52**(12), 509 (2020).
20. A. Novick et al., "High-bandwidth density silicon photonic resonators for energy-efficient optical interconnects," *Appl. Phys. Rev.* **10**(4), 041306 (2023).
21. R. Guo et al., "High-Q silicon microring resonator with ultrathin sub-wavelength thicknesses for sensitive gas sensing," *Appl. Phys. Rev.* **11**(2), 021417 (2024).
22. R. K. Lau et al., "Octave-spanning mid-infrared supercontinuum generation in silicon nanowaveguides," *Opt. Lett.* **39**(15), 4518–4521 (2014).
23. N. Nader et al., "Versatile silicon-waveguide supercontinuum for coherent mid-infrared spectroscopy," *APL Photonics* **3**(3), 036102 (2018).
24. R. Kou et al., "Mid-IR broadband supercontinuum generation from a suspended silicon waveguide," *Opt. Lett.* **43**(6), 1387–1390 (2018).
25. S. K. Boukar et al., "Supercontinuum generation of Airy pulses in a silicon-on-insulator optical waveguide including third-harmonic generation and negative-frequency Kerr terms," *Eur. Phys. J. D* **78**(7), 87 (2024).
26. N. Singh et al., "Midinfrared supercontinuum generation from 2 to 6 μm in a silicon nanowire," *Optica* **2**(9), 797–802 (2015).
27. N. Singh et al., "Octave-spanning coherent supercontinuum generation in silicon on insulator from 1.06 mum to beyond 2.4 mum," *Light Sci. Appl.* **7**, 17131 (2018).
28. A. Ishizawa et al., "Octave-spanning supercontinuum generation at telecommunications wavelengths in a precisely dispersion- and length-controlled silicon-wire waveguide with a double taper structure," *Appl. Phys. Lett.* **111**(2), 021105 (2017).
29. N. Singh et al., "Supercontinuum generation in varying dispersion and birefringent silicon waveguide," *Opt. Express* **27**(22), 31698–31712 (2019).
30. A. D. Torre et al., "Mid-infrared supercontinuum generation in a varying dispersion waveguide for multi-species gas spectroscopy," *IEEE J. Sel. Top. Quantum Electron.* **29**, 1–9 (2023).
31. J. Wei et al., "Supercontinuum generation assisted by wave trapping in dispersion-managed integrated silicon waveguides," *Phys. Rev. Appl.* **14**(5), 054045 (2020).
32. H. Zia et al., "Ultraefficient on-chip supercontinuum generation from sign-alternating-dispersion waveguides," *Adv. Photonics Res.* **4**(5), 2200296 (2023).
33. C.-Y. Lee et al., "Inverse design of coherent supercontinuum generation using free-form nanophotonic waveguides," *APL Photonics* **9**(6), 066108 (2024).
34. D. D. Hickstein et al., "Quasi-phase-matched supercontinuum generation in photonic waveguides," *Phys. Rev. Lett.* **120**(5), 053903 (2018).
35. N. Singh et al., "Supercontinuum generation in silicon Bragg grating waveguide," *Appl. Phys. Lett.* **118**(7), 071106 (2021).
36. B. B. Zhou et al., "Parametrically tunable soliton-induced resonant radiation by three-wave mixing," *Phys. Rev. Lett.* **118**(14), 143901 (2017).

Hongzhi Xiong is pursuing a PhD at the College of Optical Science and Engineering, Zhejiang University, Hangzhou, China. His current research interests include nonlinear optics and silicon photonics.

Xinmin Yao is pursuing a PhD at the College of Optical Science and Engineering, Zhejiang University, Hangzhou, China. His research interests include nonlinear optics.

Qingrui Yao is pursuing a PhD at the College of Optical Science and Engineering, Zhejiang University, Hangzhou, China. Her current research interests include silicon photonics.

Qingbo Wu is pursuing a PhD at the College of Optical Science and Engineering, Zhejiang University, Hangzhou, China. His current research interests include silicon photonics.

Hongyuan Cao is pursuing a PhD at the College of Optical Science and Engineering, Zhejiang University, Hangzhou, China. His research interests include silicon photonics and nonlinear optics materials.

Yaoxin Bao is pursuing a PhD at the College of Optical Science and Engineering, Zhejiang University, Hangzhou, China. Her research interests include silicon photonics and Raman amplifiers.

Fei Huang is pursuing a PhD at the College of Optical Science and Engineering, Zhejiang University, Hangzhou, China. His current research interests include optical frequency combs.

Zejie Yu is an associate professor at Zhejiang University, Hangzhou, China, and mainly works on integrated photonics.

Ming Zhang is an associate professor at Zhejiang University, Ningbo Research Institute, Ningbo, China, and mainly works on integrated photonics.

Daoxin Dai is a QIUSHI Distinguished Professor at Zhejiang University, Hangzhou, China, and mainly works on silicon photonics. He has published several refereed papers in international journals. He was one of the most cited Chinese researchers from 2015 to 2021 (Elsevier).